Catalysis Today 181 (2012) 133–137

Contents lists available at ScienceDirect

Catalysis Today

journal homepage: www.elsevier.com/locate/cattod

Size effect of RhPt bimetallic nanoparticles in catalytic activity of CO oxidation: Role of surface segregation

Jeong Y. Park[a], Yawen Zhang[b], Sang Hoon Joo[c], Yousung Jung[a], Gabor A. Somorjai[d,*]

[a] Graduate School of EEWS (WCU) and NanoCentury KI, KAIST, Daejeon, Republic of Korea
[b] College of Chemistry and Molecular Engineering, and the State Key Laboratory of Rare Earth Materials Chemistry and Applications & PKU-HKU Joint Laboratory in Rare Earth Materials and Bioinorganic Chemistry, Peking University, Beijing 100871, China
[c] School of Nano-Bioscience and Chemical Engineering and KIER-UNIST Advanced Center for Energy, Ulsan National Institute of Science and Engineering (UNIST), UNIST-gil 50, Ulsan 689-798, Republic of Korea
[d] Department of Chemistry, University of California, Berkeley, CA 94720, United States

ARTICLE INFO

Article history:
Received 3 March 2011
Received in revised form 14 May 2011
Accepted 30 May 2011
Available online 2 July 2011

Keywords:
CO oxidation
RhPt bimetallic nanoparticles
Size
Surface segregation

ABSTRACT

We show that catalytic activity of bimetallic $Rh_{0.5}Pt_{0.5}$ nanoparticle arrays under CO oxidation can be tuned by varying the size of nanoparticles. The tuning of size of RhPt nanoparticles was achieved by changing the concentration of rhodium and platinum precursors in one-step polyol synthesis. We obtained two dimensional $Rh_{0.5}Pt_{0.5}$ bimetallic nanoparticle arrays in size between 5.7 nm and 11 nm. CO oxidation was carried out on these two-dimensional nanoparticle arrays, revealing higher activity on the smaller nanoparticles compared to the bigger nanoparticles. X-ray photoelectron spectroscopy (XPS) results indicate the preferential surface segregation of Rh compared to Pt on the smaller nanoparticles, which is consistent with our thermodynamic analysis. Because the catalytic activity is associated with differences in the rates of O_2 dissociative adsorption between Pt and Rh, we suppose that the surface segregation of Rh on the smaller bimetallic nanoparticles is responsible for the higher catalytic activity in CO oxidation. This result suggests a control mechanism of catalytic activity via synthetic approaches for colloid nanoparticles, with possible application in rational design of nanocatalysts.

1. Introduction

The colloid nanoparticles with stabilizing agents permit us to control the size, composition, and shape that are required to precisely quantify chemical influences [1–4]. The concept of smart design of catalytic materials using bimetallic nanoparticles has drawn much interest due to the potential for enhanced activity and lower cost [5–7]. In situ characterization on bimetallic nanoparticles has been carried out to elucidate the compositional change under reaction conditions [8,9].

The CO oxidation reaction over transition metals has been a widely studied surface catalyzed reaction [10–12]. The CO oxidation reaction is of practical importance for the control of pollution that results from combustion processes. The catalytic activity for CO oxidation over transition metal surfaces is determined by the propensity for the metal surface to dissociate oxygen molecules and by the bond strength of the active oxygen species on the metal surface. This behavior is reflected in a well-known volcano curve for transition metals [13]. The transition metals with half-filled d-bands such as Pt, Pd, and Rh reveal high activity, where the dissociation probability is not too low and the adsorption energy is not too high. The size dependence of nanoparticles on the activity of CO oxidation has been reported, and the origin of the size effect has been discussed [14–20]. Recently, a variety of surface oxides have been reported to evolve on late transition metals when the pressure of oxygen is increased from ultrahigh vacuum (UHV) to one atmosphere. Recent experiments carried out at in situ conditions revealed that the oxidation state and type of surface oxide formed on the surface of these catalysts greatly affects CO oxidation rates [12,18,21,22]. These oxides attribute to the size dependence of Pd nanoparticles on the activity of CO oxidation [16]. Although extensive studies were carried out over monometallic nanoparticles, the size dependence has been rarely reported over bimetallic nanocatalysts [23].

In this study, we show the influence of size of $Rh_{0.5}Pt_{0.5}$ bimetallic nanoparticle arrays on the activity of CO oxidation. The size was controlled using colloidal chemistry with good monodispersity at a range of size between 5.7 nm and 11 nm. We found that the activity increases as the size of bimetallic nanoparticles decreases. X-ray photoelectron spectroscopy (XPS) studies on nanoparticle arrays reveal the preferential surface segregation of Pt on bigger nanoparticles. We carried out the thermodynamic analysis to understand the trend of surface energy variation of bimetallic nanoparticles.

* Corresponding author.
E-mail address: somorjai@berkeley.edu (G.A. Somorjai).

0920-5861/$ – see front matter © 2011 Elsevier B.V. All rights reserved.
doi:10.1016/j.cattod.2011.05.031

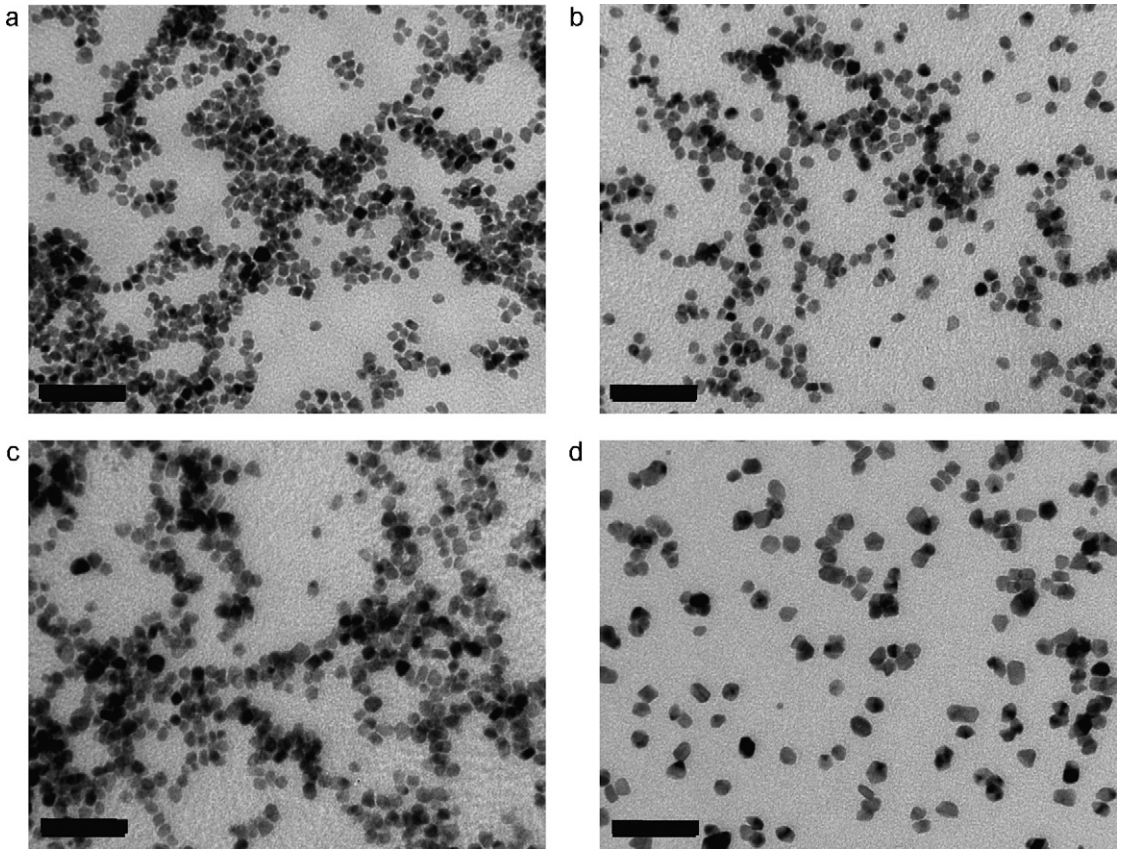

Fig. 1. TEM images of $Rh_{0.5}Pt_{0.5}$ nanocrystals with different sizes (a) 5.7 nm, (b) 6.8 nm, (c) 8.5 nm, and (d) 11.0 nm. The scale bars represent 50 nm.

2. Experimental details

2.1. Synthesis of bimetallic nanoparticles

In a typical synthesis of $Rh_{0.5}Pt_{0.5}$ binary nanoparticles, a stoichiometric amount of rhodium(III) acetylacetonate ($Rh(acac)_3$, 97%, Sigma–Aldrich), platinum acetylacetonate ($Pt(acac)_2$, 97%, Sigma–Aldrich) and poly(vinylpyrrolidone) (PVP, M_w = 55,000, Sigma–Aldrich) (in terms of the repeating unit) at a fixed (Rh + Pt)/PVP ratio of 1:10, were added to 20 mL of 1,4-butanediol (99%, Sigma–Aldrich) in a 50 mL three-necked flask at room temperature. The stock solution was heated to 140 °C in a Glas-Col electromantle (60 W; 50 mL) with a Cole-Parmer temperature controller (Diqi-sense®), and was evacuated at this temperature for 20 min to remove water and oxygen while using magnetic stirring, resulting in an optically transparent orange-yellow solution. The flask was then heated to the desired reaction temperature (in this instance, 140 °C at a rate of 10 °C min^{-1}, and maintained at this temperature for 1–2 h under Ar. During the reaction, the color of the solution gradually turned from orange-yellow to black. When the reaction was complete, an excess of acetone was poured into the solution at room temperature to form a cloudy black suspension.

This suspension was separated by centrifugation at 4200 rpm for 6 min, and the black product was collected after discarding the colorless supernatant. The precipitated Rh_xPt_{1-x} nanocrystals were washed with acetone once then re-dispersed in ethanol. The synthetic parameters for all of the nanoparticles used in this experiment are listed in Table 1. The shape, size, and lattice structure of the $Rh_{0.5}Pt_{0.5}$ nanocrystals were analyzed using a Philips FEI Tecnai 12 (conventional TEM) and Philips CM200/FEG (HRTEM), operated at 100 and 200 kV, respectively. The samples were prepared by placing a drop of a $Rh_{0.5}Pt_{0.5}$ nanocrystal sol in ethanol onto a continuous carbon-coated copper TEM grid. Fig. 1 shows TEM images of (a) 5.7 nm, (b) 6.8 nm, (c) 8.5 nm, and (d) 11.0 nm $Rh_{0.5}Pt_{0.5}$ bimetallic nanoparticles.

2.2. Preparation of Langmuir–Blodgett nanoparticle arrays

For preparing two dimensional nanoparticle arrays, the $Rh_{0.5}Pt_{0.5}$ nanocrystals were washed four times by precipitation/dissolution in ethanol and then in chloroform (1 mL of $Rh_{0.5}Pt_{0.5}$ dispersion was precipitated by adding 4 mL of hexane, and re-dispersed in 1 mL of ethanol or chloroform with sonication), to remove the impurities and excess PVP. Monolayers of $Rh_{0.5}Pt_{0.5}$ nanocrystals were formed by placing drops of $Rh_{0.5}Pt_{0.5}$ nanocrystal chloroform solution onto the water subphase of a Langmuir–Blodgett (LB) trough (Nima Technology, M611) at room temperature. The surface pressure was monitored with a Wilhelmy plate, and was adjusted to zero before spreading the nanocrystals. The resulting surface layer was compressed by moving the mobile barrier at a rate of 15 cm^2/min. The $Rh_{0.5}Pt_{0.5}$ nanocrystals were deposited onto Si wafers (0.5 cm × 1 cm) by lift-up of the substrates at a rate of 1 mm/min. XPS spectra were taken on a 15 kV, 350 W PHI 5400 ESCA/XPS system equipped with an Al anode X-ray source.

Table 1
Synthetic conditions and size of $Rh_{0.5}Pt_{0.5}$ nanocrystals.

Sample	$Pt(acac)_2$ [mmol]	$Rh(acac)_3$ [mmol]	T [°C]	t [h]	Size[a] [nm]
$Rh_{0.5}Pt_{0.5}$	0.0125	0.0125	220	2	5.7 ± 0.7
$Rh_{0.5}Pt_{0.5}$	0.00625	0.00625	220	2	6.8 ± 0.6
$Rh_{0.5}Pt_{0.5}$	0.05	0.05	220	2	8.5 ± 1.1
$Rh_{0.5}Pt_{0.5}$	0.1	0.1	220	2	11.0 ± 1.7

[a] The standard deviation from a 150 nanocrystal sample.

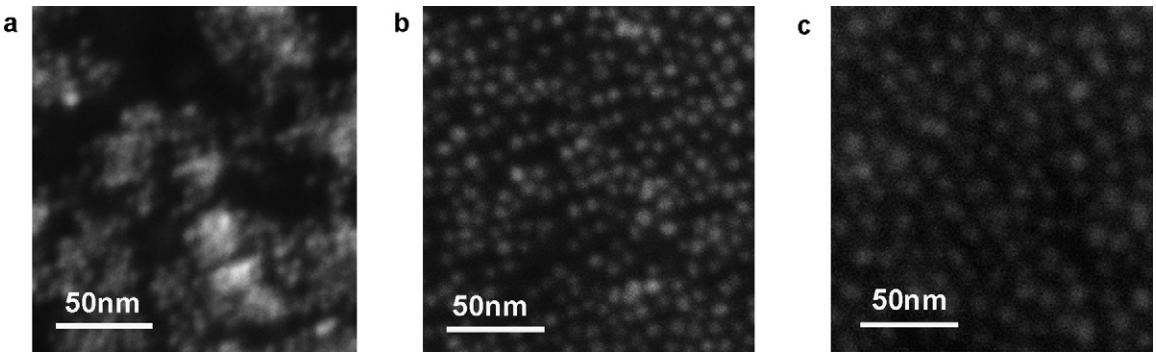

Fig. 2. SEM images of two dimensional $Rh_{0.5}Pt_{0.5}$ bimetallic nanoparticle arrays on silicon surface with variable sizes. (a) 5.7 nm, (b) 8.5 nm, and (c) 11 nm.

The number of metal sites was calculated by geometrical considerations based on scanning electron microscopy (SEM) measurements of surface area of a nanoparticle array. In this simplified estimation of the number of metal sites, we did not consider the influence of partial oxidation and bonding between metal atoms and capping layers. Fig. 2 shows SEM images of two dimensional $Rh_{0.5}Pt_{0.5}$ bimetallic nanoparticle arrays on silicon surface with variable sizes. [(a) 5.7 nm, (b) 8.5 nm, and (c) 11 nm.]

2.3. Catalytic reaction

The details about the catalytic reactor are described elsewhere [24]. The reaction cell was evacuated down to 5×10^{-8} Torr by a turbo molecular pump. A ceramic heater was used to heat the sample. The gases were circulated through the reaction line by a Metal Bellows recirculation pump at a rate of 2 L/min. An HP Series II gas chromatograph equipped with a thermal conductivity detector and a 150, 1/800 SS 60/80 Carboxen-1000 (Supelco) was used to separate the products for analysis.

CO oxidation studies were carried out in a batch reaction system under 40 Torr CO, 100 Torr O_2, and 620 Torr He. The measured reaction rates are reported as turnover frequencies (TOF) and are measured in units of product molecules of CO_2 produced per metal surface site per second of reaction time. Because all of the nanoparticles are capped with PVP, we assumed that the influence of the capping layer on all of the nanoparticles was the same [25,26].

3. Results and discussion

The catalytic oxidation of CO to CO_2 takes place in two main temperature regimes. Below the ignition temperature, CO and O combine on the platinum surface and desorb as CO_2. The reaction follows Langmuir–Hinshelwood (L–H) kinetics and the dominant surface species on platinum during reaction is CO [27,28]. Above the ignition temperature, the surface is mainly covered by oxygen adatoms. We monitored reaction kinetics of Rh_xPt_{1-x} nanocrystals by gas chromatography.

It has been found that the catalytic activity of CO oxidation by $Rh_{0.5}Pt_{0.5}$ bimetallic nanoparticles can be changed by varying the composition at a constant size (9 ± 1) nm. CO oxidation rates that exhibit a 20-fold increase from pure Pt to pure Rh show an increase with surface composition of the bimetallic nanoparticles [29]. Higher activity of Rh compared to Pt nanoparticles was attributed to the large differences in the rates of O_2 dissociative adsorption. The initial dissociative sticking probability of 0.2 on Pt and 1.0 on Rh were reported [30,31]. During the low-temperature competitive adsorption of CO and O_2 (below ignition temperature), this difference in the sticking coefficients will result in a more efficient formation of adsorbed oxygen molecules on the vacant sites of the Rh surface than on Pt, leading to faster subsequent formation of vacant sites via the reaction between neighboring adsorbed oxygen and adsorbed CO.

Fig. 3 shows the change of turnover rate on $Rh_{0.5}Pt_{0.5}$ bimetallic nanoparticle arrays measured at 180 °C and 200 °C. Over the size range of 5.7–11 nm, the smaller nanoparticle shows a 5 fold increase in turnover rate than the bigger nanoparticle. This trend is similar with Rh nanoparticles. An approximate negative-order dependence on CO and a positive order dependence on O_2 over Rh_xPt_{1-x} nanoparticles were observed at 200 °C, as shown in Fig. 4. Because the ignition temperature is 290–300 °C for Pt nanoparticles [32], this measurement was carried out below the ignition temperature. A negative-order dependence on CO and a positive order dependence on O_2 are consistent with the result of Pt (1 1 1) [10,33] as well as Rh (1 1 1) and Rh (1 0 0) [34,35].

The size dependence of $Rh_{0.5}Pt_{0.5}$ nanoparticles on the turnover rate of CO oxidation can be associated with the surface segregation effect. Fig. 5 shows the XPS spectrum of $Rh_{0.5}Pt_{0.5}$ with three different sizes of 5.5 nm, 8.5 nm, and 11 nm. It is noticeable that the ratio of Pt4d to Rh3d increases slightly as the size of the nanoparticles increases. Using the sensitivity factors of Rh and Pt and the integrated peak areas of Rh3d and Pt4f, the alloy compositions were estimated as a function of the size of the nanoparticles. We obtained $Rh_{0.47}Pt_{0.53}$, $Rh_{0.48}Pt_{0.52}$, and $Rh_{0.52}Pt_{0.48}$, for 11 nm, 8.5 nm, and 5.5 nm, respectively. The composition error, which is less than 1%, was extracted from the noise level of XPS signals of Pt and Rh (Pt 4f and Rh 3d peaks). Considering the mean free path of a photoelectron is approximately 2 nm, the result indicates that there may be a preferential segregation of Rh on the smaller $Rh_{0.5}Pt_{0.5}$ bimetallic nanoparticles. The latter result may seem counterintuitive since the surface energy [36] of the bulk Rh, 2.70 J m^{-2}, is higher than that of Pt, 2.48 J m^{-2}. However, surface energies of nanoparticles are, in general, different from the corresponding bulk materials [37].

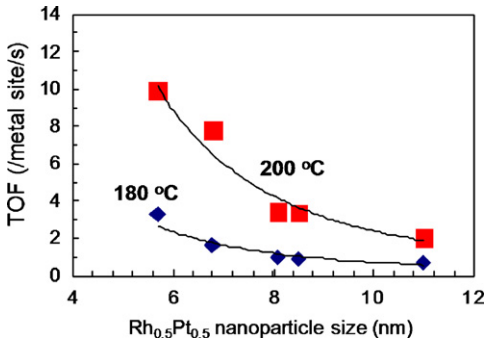

Fig. 3. Turnover rate and activation energy measured on $Rh_{0.5}Pt_{0.5}$ nanoparticles as a function of size of nanoparticles.

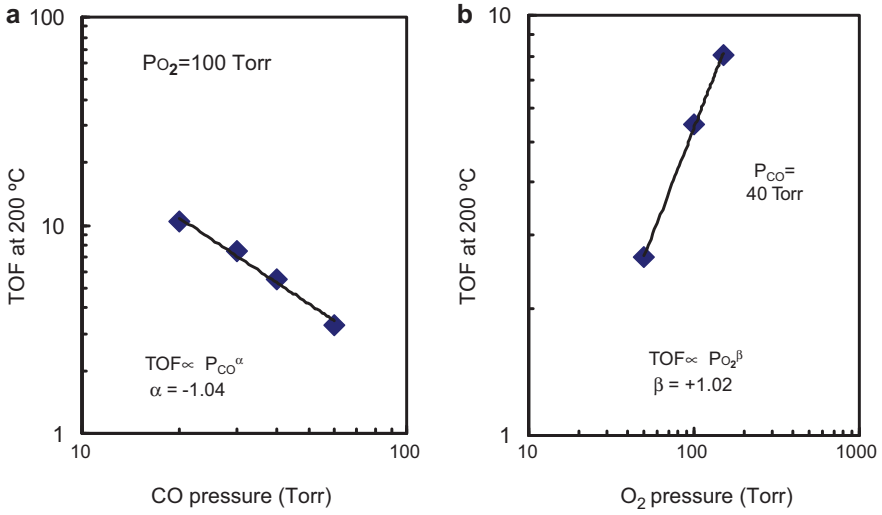

Fig. 4. Reaction order of CO oxidation on $Rh_{0.5}Pt_{0.5}$ (at 200 °C) for (a) CO and (b) O_2. α and β were obtained from the equation of TOF = (constant) × P_{CO}^{α} × P_{O2}^{β}.

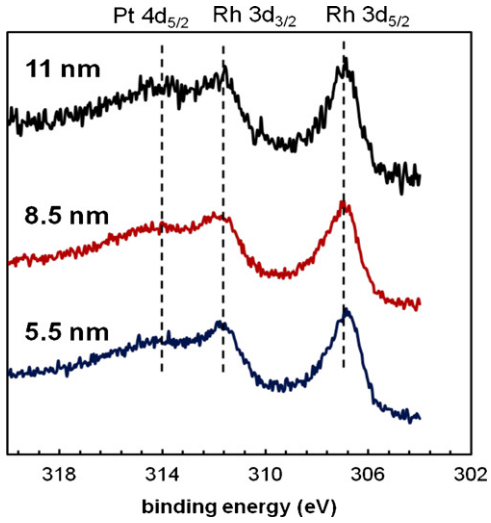

Fig. 5. XPS of Rh3d and Pt 4d peaks measured on $Rh_{0.5}Pt_{0.5}$ with three different sizes of 5.5 nm, 8.5 nm, and 11 nm.

Specifically, a simple thermodynamic analysis [38,39] suggests that the size-dependent surface energy $\gamma(D)$ can be expressed as

$$\gamma(D) = \gamma_0 \left(1 - \frac{1}{2D/h - 1}\right) \exp\left(-\frac{2S_b}{3R}\frac{1}{2D/h - 1}\right) \quad (1)$$

where D is the diameter of the nanocrystal, γ_0 is the surface energy of the bulk material, h is the atomic diameter, S_b is the cohesive entropy of the bulk material defined as $S_b = E_b/T_b$, with E_b denoting the bulk cohesive energy and T_b denoting the solid–vapor transition temperature, and R is the gas constant. Eq. (1) has no adjustable fitting parameters and only requires intrinsic thermodynamic and physical properties of the materials to evaluate. Eq. (1) is derived by and consistent with an experimental observation that the cohesive energy of nanocrystals, and hence the surface energy $\gamma(D)$, decreases with decreasing particle sizes where the rate of decrease depends on the bulk cohesive energy, solid–vapor transition temperature, and atomic size of constituents [40]. In Fig. 6a, $\gamma(D)$ for Pt and Rh are plotted as a function of $1/D$ showing different slopes of decrease in surface energy for different metals.

The inversion of relative surface energies for Pt and Rh then occurs around $D = 4$ nm, below which it means that Rh has a lower surface energy than Pt and, hence, the nanoparticle surface would be Rh-richer for the equimolar bulk concentrations of Pt and Rh. In Fig. 6b, we calculated the relative surface concentration of Rh, as compared to Pt, for the experimental range of nanoparticle sizes using an approximate Boltzmann relation:

$$\frac{x_{Rh}}{x_{Pt}} = \exp\left[\frac{-a(\gamma_{Rh}(D) - \gamma_{Pt}(D))}{RT}\right] \quad (2)$$

where x_{Rh} and x_{Pt} are the surface concentrations of Rh and Pt, respectively; a is the average area per atom; and $\gamma_{Rh}(D)$ and $\gamma_{Pt}(D)$ are the size-dependent surface energies of Rh and Pt, respectively,

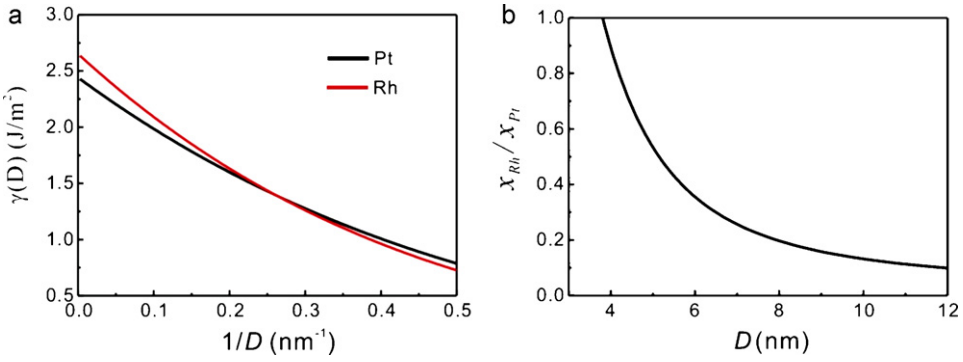

Fig. 6. (a) $\gamma(D)$ as a function of inverse particle size ($1/D$) using Eq. (1) for Pt and Rh. Parameters used in Eq. (1) are: [41] $h = 0.402$ nm, $E_b = 564$ kJ/mol, $T_b = 4908$ K for Pt, and $h = 0.387$ nm, $E_b = 554$ kJ/mol, $T_b = 3968$ K for Rh. (b) Theoretical surface concentration of Rh relative to Pt as a function of particle size using Eq. (2), assuming the bulk concentrations Pt:Rh = 50:50. Due to using an analytical expression, Eq. (1), there is no error bar in theoretical estimates.

as defined in Eq. (1). The computed size-dependent surface concentration of Rh in Fig. 6b shows a strong correlation with the experimental size-dependent activity measurements in Fig. 3. In particular, our theoretical analysis predicts that the nanoparticles with $D = 5.7$ nm would have a 3-fold increase in the Rh surface concentration (x_{Rh}) at the surface when compared to those with $D = 11$ nm. Therefore, a simple thermodynamic consideration of size-dependent surface segregation seems to offer a reasonable explanation for the observed catalytic trend. We note that, in our treatment, we have neglected the effects of possible changes in electronic structure of nanoparticles due to alloying and the potential adsorbate-induced surface segregation. As we estimate the TOF of bimetallic nanoparticles using the simplified model [29], $TOF = x_{Pt} \cdot TOF_{Pt} + x_{Rh} \cdot TOF_{Rh}$. The higher Rh concentration on smaller bimetallic nanoparticles leads to a three-fold increase in catalytic activity. Because we observed a five-fold increase in catalytic activity (Fig. 3), we suppose that other portion of increase (~5/3) would be attributed to other factors, such as the oxidation state or electronic structure of nanoparticles due to alloying and the potential adsorbate-induced surface segregation. In situ surface characterization, including XPS [9,18] or scanning probe microscopy [42] of colloid nanoparticles, would facilitate a better understanding of the change of composition, oxidation states, and structural change on the nanoparticle surface, and show the exclusive role of surface segregation. Our observation reveals the difference of TOF by a factor of 5, which is much bigger than the variation of TOF (20–30%) due to different capping layers [25]. Therefore, we suppose capping layers have a minor effect, while the change of surface composition plays a major role in determining catalytic activity. Our experiments suggest the importance of surface segregation of the catalyst surface, which demonstrates a strategy to control the catalytic activity via nanoparticles synthesis, composition and size.

4. Conclusions

We found that size of $Rh_{0.5}Pt_{0.5}$ bimetallic nanoparticle arrays can be used to tune the activity of CO oxidation. The size was synthetically varied with colloidal chemistry. We found that the catalytic activity of CO oxidation increases as the size of the bimetallic nanoparticles decreases. Thermodynamic analysis and XPS measurement suggest that the higher catalytic activity of smaller bimetallic nanoparticles is associated with the preferential surface segregation of Rh compared to Pt on the smaller nanoparticles. This result suggests the intriguing capability of changing the catalytic activity in a bimetallic nanoparticle via varying the composition and size, with possible application in tunable nanocatalysts.

Acknowledgements

This work was supported by the Director, Office of Science, Office of Basic Energy Sciences, Division of Materials Sciences and Engineering of the U.S. Department of Energy under contract no. DE-AC02-05CH11231. J.Y.P. and Y.S.J. acknowledges the support by WCU program through the National Research Foundation of Korea (31-2008-000-10055-0) and by a grant from the Fundamental R&D Program for Core Technology of Materials funded by the Ministry of Knowledge Economy, Republic of Korea. S.H.J. was supported by Basic Science Research Program through the National Research Foundation of Korea funded by the Ministry of Education, Science and Technology (2010-0005341) and by TJ Park Junior Faculty Fellowship.

References

[1] R. Narayanan, M.A. El-Sayed, Nano Letters 4 (2004) 1343.
[2] K.M. Bratlie, H. Lee, K. Komvopoulos, P. Yang, G.A. Somorjai, Nano Letters 7 (2007) 3097.
[3] G.A. Somorjai, J.Y. Park, Angewandte Chemie-International Edition 47 (2008) 9212.
[4] G.A. Somorjai, F. Tao, J.Y. Park, Topics in Catalysis 47 (2008) 1.
[5] J.K. Norskov, T. Bligaard, J. Rossmeisl, C.H. Christensen, Nature Chemistry 1 (2009) 37.
[6] N. Toshima, T. Yonezawa, New Journal of Chemistry 22 (1998) 1179.
[7] R. Ferrando, J. Jellinek, R.L. Johnston, Chemical Reviews 108 (2008) 845.
[8] V.R. Stamenkovic, B.S. Mun, M. Arenz, K.J.J. Mayrhofer, C.A. Lucas, G.F. Wang, P.N. Ross, N.M. Markovic, Nature Materials 6 (2007) 241.
[9] F. Tao, M.E. Grass, Y.W. Zhang, D.R. Butcher, J.R. Renzas, Z. Liu, J.Y. Chung, B.S. Mun, M. Salmeron, G.A. Somorjai, Science 322 (2008) 932.
[10] X.C. Su, P.S. Cremer, Y.R. Shen, G.A. Somorjai, Journal of the American Chemical Society 119 (1997) 3994.
[11] D.W. Goodman, Chemical Reviews 95 (1995) 523.
[12] H. Over, Y.D. Kim, A.P. Seitsonen, S. Wendt, E. Lundgren, M. Schmid, P. Varga, A. Morgante, G. Ertl, Science 287 (2000) 1474.
[13] J. Greeley, J.K. Norskov, M. Mavrikakis, Annual Review of Physical Chemistry 53 (2002) 319.
[14] M. Haruta, S. Tsubota, T. Kobayashi, H. Kageyama, M.J. Genet, B. Delmon, Journal of Catalysis 144 (1993) 175.
[15] M. Valden, X. Lai, D.W. Goodman, Science 281 (1998) 1647.
[16] M.S. Chen, Y. Cal, Z. Yan, K.K. Gath, S. Axnanda, D.W. Goodman, Surface Science 601 (2007) 5326.
[17] D.C. Lim, I. Lopez-Salido, Y.D. Kim, Surface Science 598 (2005) 96.
[18] M.E. Grass, Y.W. Zhang, D.R. Butcher, J.Y. Park, Y.M. Li, H. Bluhm, K.M. Bratlie, T.F. Zhang, G.A. Somorjai, Angewandte Chemie-International Edition 47 (2008) 8893.
[19] S.H. Joo, J.Y. Park, J.R. Renzas, D.R. Butcher, W.Y. Huang, G.A. Somorjai, Nano Letters 10 (2010) 2709.
[20] N. Lopez, T.V.W. Janssens, B.S. Clausen, Y. Xu, M. Mavrikakis, T. Bligaard, J.K. Norskov, Journal of Catalysis 223 (2004) 232.
[21] M.D. Ackermann, T.M. Pedersen, B.L.M. Hendriksen, O. Robach, S.C. Bobaru, I. Popa, C. Quiros, H. Kim, B. Hammer, S. Ferrer, J.W.M. Frenken, Physical Review Letters (2005) 95.
[22] A.J. Nagy, G. Mestl, R. Schlogl, Journal of Catalysis 188 (1999) 58.
[23] Q.S. Liu, Z. Yan, N.L. Henderson, J.C. Bauer, D.W. Goodman, J.D. Batteas, R.E. Schaak, Journal of the American Chemical Society 131 (2009) 5720.
[24] J.Y. Park, J.R. Renzas, B.B. Hsu, G.A. Somorjai, Journal of Physical Chemistry C 111 (2007) 15331.
[25] J.Y. Park, C. Aliaga, J.R. Renzas, H. Lee, G.A. Somorjai, Catalysis Letters 129 (2009) 1.
[26] C. Aliaga, J.Y. Park, Y. Yamada, H.S. Lee, C.K. Tsung, P.D. Yang, G.A. Somorjai, Journal of Physical Chemistry C 113 (2009) 6150.
[27] G.A. Somorjai, Introduction to Surface Chemistry and Catalysis, Wiley, New York, 1994.
[28] T. Engel, G. Ertl, Journal of Chemical Physics 69 (1978) 1267.
[29] J.Y. Park, Y. Zhang, M. Grass, T. Zhang, G.A. Somorjai, Nano Letters 8 (2008) 673.
[30] W.M. Daniel, Y. Kim, H.C. Peebles, J.M. White, Surface Science 111 (1981) 189.
[31] C.R. Helms, H.P. Bonzel, S. Kelemen, Journal of Chemical Physics 65 (1976) 1773.
[32] S.H. Joo, J.Y. Park, C.K. Tsung, Y. Yamada, P.D. Yang, G.A. Somorjai, Nature Materials 8 (2009) 126.
[33] N.W. Cant, P.C. Hicks, B.S. Lennon, Journal of Catalysis 54 (1978) 372.
[34] C.H.F. Peden, D.W. Goodman, D.S. Blair, P.J. Berlowitz, G.B. Fisher, S.H. Oh, Journal of Physical Chemistry 92 (1988) 1563.
[35] S.B. Schwartz, L.D. Schmidt, G.B. Fisher, Journal of Physical Chemistry 90 (1986) 6194.
[36] F.R. de Boer, R. Boom, W.C.M. Mattens, A.R. Miedema, A.K. Niessen, Cohesion in Metals, North-Holland, Amsterdam, 1988.
[37] G. Ouyang, C.X. Wang, G.W. Yang, Chemical Reviews 109 (2009) 4221.
[38] Q. Jiang, H.M. Lu, Surface Science Reports 63 (2008) 427.
[39] X.C. Zhou, W.L. Xu, G.K. Liu, D. Panda, P. Chen, Journal of the American Chemical Society 132 (2010) 138.
[40] Q. Jiang, J.C. Li, B.Q. Chi, Chemical Physics Letters 366 (2002) 551.
[41] http://www.webelements.com.
[42] J.Y. Park, Langmuir 27 (2011) 2509–2513.